AERO-ASTRONAUTICS REPORT NO. 242

OPTIMAL TRAJECTORIES
FOR THE AEROASSISTED FLIGHT EXPERIMENT,
PART 3, FORMULATION, RESULTS, AND ANALYSIS

by

A. MIELE, T. WANG, W. Y. LEE, AND Z. G. ZHAO

RICE UNIVERSITY

1989

OPTIMAL TRAJECTORIES

FOR THE AEROASSISTED FLIGHT EXPERIMENT,

PART 3, FORMULATION, RESULTS, AND ANALYSIS

by

A. MIELE, T. WANG, W. Y. LEE, AND Z. G. ZHAO

RICE UNIVERSITY

1989

Optimal Trajectories

for the Aeroassisted Flight Experiment,

Part 3, Formulation, Results, and Analysis[1,2]

by

A. Miele[3], T. Wang[4], W. Y. Lee[5], and Z. G. Zhao[6]

[3]Foyt Family Professor of Aerospace Sciences and Mathematical Sciences, Aero-Astronautics Group, Rice University, Houston, Texas.

[4]Senior Research Scientist, Aero-Astronautics Group, Rice University, Houston, Texas.

[5]Post-Doctoral Fellow, Aero-Astronautics Group, Rice University, Houston, Texas.

[6]Research Associate, Aero-Astronautics Group, Rice University, Houston, Texas.

Abstract. This report is the third of a series (Refs. 1-4) dealing with the determination of optimal trajectories for the aero-assisted flight experiment (AFE). The intent of this experiment is to simulate a GEO-to-LEO transfer, where GEO denotes a geosynchronous Earth orbit and LEO denotes a low Earth orbit. Specifically, the AFE spacecraft is released from the space shuttle and is accelerated by means of a solid rocket motor toward Earth, so as to achieve atmospheric entry conditions identical with those of a spacecraft returning from GEO. During the atmospheric pass, the angle of attack is kept constant, and the angle of bank is controlled in such a way that the following conditions are satisfied: (a) the atmospheric velocity depletion is such that, after exiting, the AFE spacecraft first ascends to a specified apogee and then descends to a specified perigee; and (b) the exit orbital plane is identical with the entry orbital plane. The final maneuver, not analyzed here, includes the rendezvous with and the capture by the space shuttle.

In this report, the trajectories of an AFE spacecraft are analyzed in a 3D-space, employing the full system of 6 ODEs describing the atmospheric pass. The atmospheric entry conditions are given, and the atmospheric exit conditions are adjusted in such a way that requirements   (a)   and (b) are met, while simultaneously minimizing the total characteristic velocity, hence the propellant consumption required for orbital transfer. Two possible transfers are

considered: (IA) indirect ascent to a 178 NM perigee via a 197 NM apogee; and (DA) direct ascent to a 178 NM apogee.

For both transfers, two cases are investigated: (i) the bank angle is continuously variable; and (ii) the trajectory is divided into segments along which the bank angle is constant. For case (ii), the following subcases are studied: two segments, three segments, four segments, and five segments;because the time duration of each segment is optimized, the above subcases involve four, six, eight, and ten parameters, respectively.

A surprising result of the analysis is that the optimal trajectories of cases (i) and (ii) coalesce into a single trajectory: a two-subarc trajectory, with the bank angle constant in each subarc (bang-bang control). Specifically, the bank angle is near 180 deg in the atmospheric entry phase (positive lift projection phase) and is near 0 deg in the atmospheric exit phase (negative lift projection phase). Another surprising result is that, during the atmospheric pass, the peak values of the changes of the orbital inclination and the longitude of the ascending node are nearly zero; hence, the peak value of the wedge angle (angle between the instantaneous orbital plane and the initial orbital plane) is nearly zero. This means that the motion of the spacecraft is nearly planar in an inertial space.

The guidance implications of the above results are discussed.

Key Words. Flight mechanics, hypervelocity flight, atmospheric flight, optimal trajectories, aeroassisted flight experiment, aeroassisted orbital transfer, guidance.

1. Introduction

In previous reports (Refs. 1-2), the equations of motion of an AFE vehicle were derived first in an Earth-fixed system (Ref. 1) and then in an inertial system (Ref. 2). In this report (Ref.3), the problem of the optimal trajectories is formulated, solved, and analyzed. In a subsequent report (Ref. 4), more technical details are provided in the form of data, tables, and graphs.

The aeroassisted flight experiment (AFE) refers to the study of the free flight of an autonomous spacecraft, shuttle-launched and shuttle-recovered. Its purpose is to gather atmospheric entry data for use in designing aeroassited orbital transfer vehicles (AOTV). The intent of this experiment is to simulate a GEO-to-LEO transfer, where GEO denotes a geosynchronous Earth orbit and LEO denotes a low Earth orbit (Ref. 5).

In an actual AOT tranfer, GEO-to-LEO, the maneuver is initiated with a propulsive impulse at GEO so as to decelerate the spacecraft and force it into an elliptical transfer orbit leading to atmospheric entry. In a simulated AOT transfer, GEO-to-LEO, the maneuver is initiated by releasing the spacecraft from the space shuttle, which is flying at the altitude of 160 NM above the Earth surface. By means of a solid rocket motor, the AFE spacecraft is accelerated toward Earth, so as to achieve atmospheric entry conditions identical with those of a spacecraft returning from GEO. Thus, for the purposes of this report, the atmospheric entry conditions are to be considered as given.

During the atmospheric pass, the angle of attack of the AFE spacecraft is kept at the constant value $\alpha = 17$ deg. This value is such that the lift L is negative. Control of the AFE spacecraft is achieved via the angle of bank μ. Hence, the projected lift $L_p = L\cos\mu$ (the vertical component of the lift vector) can be made positive or negative at will, depending on the value of μ.

The time history of the control, the bank angle $\mu(t)$, is subject to two requirements: (a) the atmospheric velocity depletion must be such that, after exiting, the AFE spacecraft first ascends to a specified apogee and then descends to a specified perigee; and (b) the exit orbital plane must be identical with the entry orbital plane; this is the same as stating that the exit value of the wedge angle must vanish; see Ref. 5. Here, one additional requirement is considered: (c) the propellant consumption required for orbital transfer must be as small as possible, implying that the characteristic velocity ΔV must be as small as possible; in turn, minimizing ΔV is equivalent to maximizing the exit value of the horizontal component of the inertial velocity; this implies either maximizing the exit value of the inertial velocity or minimizing the exit value of the inertial path inclination.

In this report, the optimal trajectories of the AFE spacecraft are determined with reference to a 3D-space and employing the full system of 6 ODEs describing the atmospheric pass. In the general formulation of Refs. 1-2, the effects due to the rotation of the Earth and the oblateness of the Earth are included. In this report and the subsequent report (Refs. 3-4), the former are included,

but the latter are excluded, since they have been found to be small.

The resulting optimal control problem is solved by means of the

sequential gradient-restoration algorithm (SGRA, Refs. 6-12).

While this algorithm is available in both the primal formulation

(Refs. 6-9) and the dual formulation (Refs. 10-12), the former

is used in this report, based on previous experience with various

AOT problems (Refs. 13-19).

Using SGRA, the optimal trajectories are computed for two

possible transfers: (IA) indirect ascent to a 178 NM perigee via

a 197 NM apogee; and (DA) direct ascent to a 178 NM apogee. For

each transfer, two cases are investigated: (i) the bank angle

is continuously variable; hence, $\mu(t)$ is treated as a control;

and (ii) the trajectory is divided into segments along which the

bank angle is constant; hence, for each segment, μ is treated as

a parameter. For case (ii), the following subcases are studied:

2, 3, 4, 5 segments; because the time duration of each segment is

also a parameter to be optimized, the above subcases involve 4, 6,

8, 10 parameters, respectively.

For comparison purposes and only for Transfer (IA), a reference

trajectory is also considered: this is a 5-segment trajectory,

close to the nominal trajectory given in Ref. 5.

To sum up, this report considers ten optimal trajectories,

five for Transfer (IA) and five for Transfer (DA). These optimal

trajectories are compared with (and are found to be superior to)

the reference trajectory in terms of the main quantities of

interest, namely: total characteristic velocity, peak heating rate, peak dynamic pressure, peak change of orbital inclination, peak change of the longitude of the ascending node, and peak value of the wedge angle.

The report ends with a discussion of the guidance implications of the results obtained on optimal trajectories.

Content. Section 2 contains the notations. The system description is given in Section 3, and the optimization problem is formulated in Section 4. The experimental data are given in Section 5, and the numerical results are presented in Section 6. The guidance implications of the results are discussed in Section 7, and the conclusions are given in Section 8.

2.   Notations

Throughout this report, the following notations are employed:

C_D = drag coefficient;

C_L = lift coefficient;

D   = drag, N;

g   = local acceleration of gravity, m/sec^2;

h   = altitude, m;

i   = orbital inclination, rad;

L   = lift, N;

m   = mass, kg;

r   = radial distance from the center of the Earth, m;

r_e = radius of the Earth, m;

r_a = radius of the outer edge of the atmosphere, m;

S   = reference surface area, m^2;

t   = time, sec;

V   = velocity, m/sec;

V_a = circular velocity at $r = r_a$, m/sec;

α = angle of attack, rad;

γ = path inclination, rad;

η = wedge angle, rad;

θ = longitude, rad;

μ = bank angle, rad;

μ_e = Earth's gravitational constant, m^3/sec^2;

ρ = air density, kg/m^3;

τ = final time, sec;

ϕ = latitude, rad;

χ = heading angle, rad;

ω = angular velocity of the Earth, rad/sec;

Ω = longitude of the ascending node, rad;

ΔV = characteristic velocity, m/sec.

Subscripts

0   = entry into the atmosphere;

1   = exit from the atmosphere;

11   = perigee for Transfer (IA) or apogee for Transfer (DA);

22   = apogee for Transfer (IA).

Superscripts

$\cdot$ = derivative with respect to time;

$\sim$ = quantity defined in an inertial system.

Acronyms

AFE   =   aeroassisted flight experiment;

AFEV   =   aeroassisted flight experiment vehicle;

AOT   =   aeroassisted orbital transfer;

AOTV   =   aeroassisted orbital transfer vehicle;

DA   =   direct ascent;

DP   =   dynamic pressure, N/m^2;

GEO   =   geosynchronous Earth orbit;

HEO   =   high Earth orbit;

HR   =   heating rate, W/m^2;

IA   =   indirect ascent;

LAN   = longitude of the ascending node, rad;

LEO   = low Earth orbit;

ODE   = ordinary differential equation;

OT   = optimal trajectory;

RT   = reference trajectory;

SGRA   = sequential gradient-restoration algorithm;

WA   = wedge angle, rad.

3. System Description

The motion of the AFE spacecraft takes place partly in the atmosphere and partly in space. For the purposes of this report, the initial point is the atmospheric entry point; it corresponds to GEO return conditions and is fixed; the final point is located at the altitude of 178 NM and corresponds to circularization into LEO. We consider two transfer maneuvers: (IA) indirect ascent to a 178 NM perigee via a 197 NM apogee; and (DA) direct ascent to a 178 NM apogee.

For Transfer (IA), the key points of the maneuver are these: point 0, atmospheric entry; point 1, atmospheric exit; point 22, apogee (h = 197 NM) of the first post-atmospheric transfer orbit; and point 11, perigee (h = 178 NM) of the second post-atmospheric transfer orbit. Propulsive impulses are applied at two points: at the apogee 22 in order to raise the height of the perigee; and at the perigee 11 in order to circularize the motion.

For Transfer (DA), the key points of the maneuver are these: point 0, atmospheric entry; point 1, atmospheric exit; and point 11, apogee (h = 178 NM) of the post-atmospheric transfer orbit. A propulsive impulse is applied at only one point: at the apogee 11 in order to circularize the motion.

For the atmospheric portion ($h \leq h_a$) of the trajectory of the AFE spacecraft, we employ an Earth-fixed system; for the space portion of the trajectory ($h \geq h_a$), we employ an inertial system; here, h_a = 400,000 ft $\cong$ 121.9 km denotes the thickness of the

atmosphere. For $h \leq h_a$, we compute the air density using the US Standard Atmosphere, 1976 (Ref. 20); for $h \geq h_a$, we assume that the air density is zero. For both the atmospheric portion and the space portion of the trajectory, we neglect the effects due to the oblateness of the Earth; we assume that the gravitational field is central and obeys the inverse square law.

Atmospheric Pass. With reference to the atmospheric portion of the trajectory of the AFE vehicle, the following additional hypotheses are employed: (a) the atmospheric pass is made with engine shut-off; hence, the AFE spacecraft behaves as a particle of constant mass; (b) the angle of attack is constant, $\alpha = 17$ deg; (c) under extreme hypersonic conditions, the dependence of the aerodynamic coefficients on the Mach number and the Reynolds number is disregarded; (d) the sideslip angle is zero; hence, the side force component of the aerodynamic force is zero. The only control is the angle of bank μ.

Differential System. With the above assumptions and upon using an Earth-fixed system, the equations of motion include the kinematical equations (Ref. 1)

$$\dot{\theta} = V\cos\gamma \, \cos\chi/r\cos\phi, \tag{1a}$$

$$\dot{\phi} = -V\cos\gamma \, \sin\chi/r, \tag{1b}$$

$$\dot{r} = V\sin\gamma, \tag{1c}$$

and the dynamical equations (Ref. 1)

$$\dot{V} = -D/m - g\sin\gamma$$

$$+ \omega^2 r(\sin\gamma \, \cos^2\phi + \cos\gamma \, \sin\chi \, \cos\phi \, \sin\phi), \tag{1d}$$

$$\dot{\gamma} = (L/mV)\cos\mu + (V/r - g/V)\cos\gamma + 2\omega\cos\chi\cos\phi$$

$$+ (\omega^2 r/V)(\cos\gamma\cos^2\phi - \sin\gamma\sin\chi\cos\phi\sin\phi), \tag{1e}$$

$$\dot{\chi} = (L/mV)\sin\mu/\cos\gamma + (V/r)\cos\gamma\cos\chi\tan\phi$$

$$+ 2\omega(\sin\phi + \tan\gamma\sin\chi\cos\phi)$$

$$+ (\omega^2 r/V)\cos\chi\cos\phi\sin\phi/\cos\gamma. \tag{1f}$$

In the dynamical equations, the symbol ω denotes the angular velocity of the Earth; terms linear in ω are due to the Coriolis acceleration; terms quadratic in ω are due to the transport acceleration. Also in the dynamical equations, the acceleration of gravity is given by

$$g = \mu_e/r^2, \tag{2}$$

where μ_e denotes the Earth's gravitational constant. In addition, the aerodynamic forces are given by

$$D = (1/2)C_D(\alpha)\rho(h)Sv^2, \tag{3a}$$

$$L = (1/2)C_L(\alpha)\rho(h)Sv^2, \tag{3b}$$

where the air density ρ depends on the altitude h, with

$$h = r - r_e. \tag{3c}$$

Since α is constant, both the drag coefficient and the lift coefficient are constant. The control of the spacecraft is the angle of bank μ. Equations (1) must be integrated, subject

to (2) and (3), over the time interval $0 \leq t \leq \tau$. Here, the initial time $t = 0$ corresponds to atmospheric entry; and the final time $t = \tau$ corresponds to atmospheric exit.

Transformation Relations. The following transformation relations allow one to pass from quantities computed in an Earth-fixed system to quantities computed in an inertial system, and viceversa:

$$\tilde{\theta} = \theta + \omega t, \tag{4a}$$

$$\tilde{\phi} = \phi, \tag{4b}$$

$$\tilde{r} = r, \tag{4c}$$

$$\tilde{V}\cos\tilde{\gamma}\,\cos\tilde{\chi} = V\cos\gamma\,\cos\chi + \omega r\,\cos\phi, \tag{4d}$$

$$\tilde{V}\cos\tilde{\gamma}\,\sin\tilde{\chi} = V\cos\gamma\,\sin\chi, \tag{4e}$$

$$\tilde{V}\sin\tilde{\gamma} = V\sin\gamma. \tag{4f}$$

The first three equations are linear and refer to the state variables appearing in the kinematical equations. The next three equations are nonlinear and refer to the state variables appearing in the dynamical equations; in spite of the nonlinearity, these equations can be solved explicitly to yield $\tilde{V}$, $\tilde{\gamma}$, $\tilde{\chi}$ in terms of V, γ, χ, and viceversa. This step is omitted for the sake of brevity; see Refs. 1-2.

Orbital Elements. Once the state variables are known in the inertial system, one can compute some important orbital quantities such as the orbital inclination i and the longitude of the ascending node Ω. These quantities are supplied by the relations

$$\cos i = \cos\phi \, \cos\tilde{\chi}, \tag{5a}$$

$$\sin(\tilde{\theta} - \Omega) = \cot i \, \tan\phi. \tag{5b}$$

Another important quantity is the wedge angle η, which is the angle between the instantaneous orbital plane and the entry orbital plane. This angle is given by

$$\cos\eta = \sin i \, \sin i_0 \, \cos(\Omega - \Omega_0) + \cos i \, \cos i_0. \tag{5c}$$

Summary. To sum up, in the Earth-fixed system, the equations governing the atmospheric pass include the differential system (1) and the analytical and functional relations (2)-(3). In this formulation, the independent variable is the time t, $0 \le t \le \tau$. The dependent variables include six state variables [$\theta(t)$, $\phi(t)$, $r(t)$, $V(t)$, $\gamma(t)$, $\chi(t)$], one control variable [$\mu(t)$], and one parameter (τ). If the initial values of the state variables are given and if the bank angle program is prescribed, the system can be integrated in forward time. Then, using (4), one can convert the state variables computed in the Earth-fixed system

into state variables computed in the inertial system. Finally,
using (5), one can determine the orbital inclination, the
longitude of the ascending node, and the wedge angle.

Initial Conditions. At atmospheric entry, the initial values
of the state variables $\tilde{\theta}_0$, ϕ_0, $r_0 = r_a$, $\tilde{V}_0$, $\tilde{\gamma}_0$, $\tilde{\chi}_0$ are given in
the inertial system. Hence, the initial values of the orbital
elements i_0, Ω_0 are known. By definition, the initial value of
the wedge angle satisfies the relation $\eta_0 = 0$. Using the
transformation relations (4), the initial values of the state
variables θ_0, ϕ_0, $r_0 = r_a$, V_0, γ_0, χ_0 become known in the Earth-
fixed system.

Final Conditions. The final time τ is free and is to be
determined indirectly as the time instant at which the spacecraft
exits from the atmosphere; hence,

$$r_1 = r_a. \tag{6a}$$

Application of energy conservation and angular momentum
conservation to the exit-to-apogee transfer orbit yields either
the relation

$$\text{(IA)} \quad r_{22}^2(2\tilde{V}_a^2 - \tilde{V}_1^2) - 2r_{22}r_a\tilde{V}_a^2 + r_a^2\tilde{V}_1^2\cos^2\tilde{\gamma}_1 = 0 \tag{6b}$$

or the relation

$$\text{(DA)} \quad r_{11}^2(2\tilde{V}_a^2 - \tilde{V}_1^2) - 2r_{11}r_a\tilde{V}_a^2 + r_a^2\tilde{V}_1^2\cos^2\tilde{\gamma}_1 = 0. \tag{6c}$$

Equation (6b) applies to the indirect ascent case; Equation (6c) applies to the direct ascent case. These relations guarantee that, after exiting, the spacecraft ascends to the specified apogee. Finally, the orbital plane at atmospheric exit must be identical with the orbital plane at atmospheric entry; hence, the exit value of the wedge angle must vanish,

$$\eta_1 = 0. \tag{6d}$$

Use of the transformation relations (4) in conjunction with (5) allows one to transform the final conditions (6) to include quantities computed in the Earth-fixed system.

4.   Optimal Control Problem

Subject to the previous constraints, different optimal control problems can be formulated, depending on the performance index chosen and the type of transfer maneuver considered. Here, we focus attention on the minimization of the total characteristic velocity ΔV, which is a measure of the propellant consumption required for orbital transfer.

<u>Problem (IA)</u>. This problem refers to the indirect ascent to a 178 NM perigee via a 197 NM apogee. The functional to be minimized is given by

$$I = \Delta V = \Delta V_{22} + \Delta V_{11}, \tag{7a}$$

with

$$\Delta V_{22} = \tilde{V}_a \sqrt{[2r_a r_{11}/(r_{11}r_{22} + r_{22}^2)]} - (r_a/r_{22})\tilde{V}_1 \cos\tilde{\gamma}_1, \tag{7b}$$

$$\Delta V_{11} = \tilde{V}_a \sqrt{[2r_a r_{22}/(r_{11}r_{22} + r_{11}^2)]} - \tilde{V}_a \sqrt{(r_a/r_{11})}. \tag{7c}$$

<u>Problem (DA)</u>. This problem refers to the direct ascent to a 178 NM apogee. The functional to be minimized is given by

$$I = \Delta V = \Delta V_{11}, \tag{8a}$$

with

$$\Delta V_{11} = \tilde{V}_a \sqrt{(r_a/r_{11})} - (r_a/r_{11})\tilde{V}_1 \cos\tilde{\gamma}_1. \tag{8b}$$

Alternative Formulations. Inspection of the performance indexes (7) and (8) shows that they include a constant part and a part which is linear in the exit value of the horizontal component of the inertial velocity $\tilde{V}_h = \tilde{V}\cos\tilde{\gamma}$. Hence, the minimization of ΔV is equivalent to maximizing the functional

$$J = \tilde{V}_{h1} = \tilde{V}_1\cos\tilde{\gamma}_1. \tag{9a}$$

In turn, because of the final conditions (6b) or (6c), the maximization of the functional (9a) implies either maximizing the functional

$$K = \tilde{V}_1 \tag{9b}$$

or minimizing the functional

$$H = \tilde{\gamma}_1. \tag{9c}$$

Continuous vs Discrete Control. For both Problems (IA) and (DA), two cases are investigated: continuous control and discrete control.

(i)   Continuous Control. Here, the bank angle is continuously variable. Hence, $\mu(t)$ is treated as a control variable.

(ii)   Discrete Control. Here, the trajectory is divided into s segments along which the bank angle is constant; hence, for each segment, the bank angle μ_i is treated as a parameter. Because the time duration τ_i of each segment is also a parameter to be optimized, the number of parameters is twice the number of segments. The following subcases are studied: s = 2, 3, 4, 5. These subcases involve n_p = 4, 6, 8, 10 parameters, respectively.

Algorithm. For both cases (i) and (ii), Problems (IA) and
(DA) are optimal control problems of the Bolza type. They can be
solved using the sequential gradient-restoration algorithm (SGRA),
employed in conjunction with the primal formulation (PSGRA,
Refs. 6-9).

The sequential gradient-restoration algorithm is an iterative
technique which involves a sequence of cycles, each cycle including
two phases: the gradient phase and the restoration phase. In
the gradient phase, the value of the augmented functional is
decreased, while avoiding excessive constraint violation. In
the restoration phase, the value of the constraint error is
decreased, while avoiding excessive change in the value of the
functional. In a complete gradient-restoration cycle, the value
of the functional is decreased, while the constraints are satisfied
to a preselected degree of accuracy. Thus, a succession of
suboptimal solutions is generated, each new solution being an
improvement over the previous one from the point of view of
the value of the functional being minimized.

The convergence conditions are represented by the relations

$$P \leq \epsilon_1, \qquad Q \leq \epsilon_2. \tag{10}$$

Here, P is the norm squared of the error in the constraints; Q
is the norm squared of the error in the optimality conditions;
and ϵ_1, ϵ_2 are preselected small, positive numbers.

5. Experimental Data

The following data were used in the numerical experiment (for more significant digits, see Ref. 4).

Earth's Physical Constants. The radius of the Earth is r_e = 6378 km; the radius of the outer edge of the atmosphere is r_a = 6500 km; the thickness of the atmosphere is h_a = 121.9 km; the Earth's gravitational constant is μ_e = 0.3986E+15 m^3/sec^2; the circular velocity at $r = r_a$ is $\tilde{V}_a$ = 7.831 km/sec; the angular velocity of the Earth is ω = 0.7292E-04 rad/sec.

Spacecraft Data. The mass of the AFE spacecraft is m = 1678 kg; the reference surface area is S = 14.31 m^2; the spacecraft flies at constant angle of attack, α = 17.00 deg; the lift coefficient is C_L =-0.3707; and the drag coefficient is C_D = 1.315.

Atmospheric Model. The assumed atmospheric model is that of the US Standard Atmosphere, 1976 (Ref. 20). In this model, the values of the density are tabulated at discrete altitudes. For intermediate altitudes, the density is computed by assuming an exponential fit for the function $\rho(h)$.

Heating Rate. The stagnation point heating rate is assumed to be given by the formula

$$HR = C\sqrt{(\rho/\rho_R)} \, (V/V_R)^{3.07}. \tag{11}$$

Here, ρ_R is a reference density, the density at h_R= 60 km; $V_R = \tilde{V}_a$ is a reference velocity; the constant C represents the stagnation point heating rate at $\rho = \rho_R$ and $V = V_R$ and is given by C = 282.3 W/cm^2; note that the value of this constant is based on a nose radius of one foot.

Atmospheric Entry Conditions. In the inertial system, the given initial conditions are as follows: the longitude is $\tilde{\theta}_0$ = -134.52 deg; the latitude is ϕ_0 = -4.49 deg; the altitude is h_0 = 121.9 km; the radius is r_0 = 6500 km; the velocity is $\tilde{V}_0$ = 10.31 km/sec; the path inclination is $\tilde{\gamma}_0$ = -4.49 deg; the heading angle is $\tilde{\chi}_0$ = -28.13 deg; the orbital inclination is i_0 = 28.45 deg; the longitude of the ascending node is Ω_0 = -126.19 deg; the wedge angle is η_0 = 0.00 deg.

Atmospheric Exit Conditions. In the inertial system, the desired final conditions are as follows: the altitude is h_1 = 121.9 km; the radius is r_1 = 6500 km; the orbital inclination is i_1 = 28.45 deg; the longitude of the ascending node is Ω_1 = -126.19 deg; the wedge angle is η_1 = 0.00 deg.

Transfer (IA). This is the indirect ascent to a 178 NM perigee via a 197 NM apogee. The required apogee conditions are as follows: the altitude is h_{22} = 364.8 km; the radius is r_{22} = 6743 km; and the path inclination is $\tilde{\gamma}_{22}$ = 0.00 deg. The required perigee conditions are as follows: the altitude is h_{11} = 329.7 km; the radius is r_{11} = 6708 km; and the path inclination is $\tilde{\gamma}_{11}$ = 0.00 deg.

Transfer (DA). This is the direct ascent to a 178 NM apogee. The required apogee conditions are as follows: the altitude is h_{11} = 329.7 km; the radius is r_{11} = 6708 km; and the path inclination is $\tilde{\gamma}_{11}$ = 0.00 deg.

6.   Numerical Results

The optimal control problem formulated in Sections 3-4
was solved with the sequential gradient-restoration algorithm
for the experimental data outlined in Section 5. Both Transfer
(IA) and Transfer (DA) were optimized from the point of view of
the characteristic velocity ΔV. For each transfer, five optimal
trajectories (OT) were computed: the continuous control OT; the
discrete control OT with $s = 2$ segments; the discrete control OT
with $s = 3$ segments; the discrete control OT with $s = 4$ segments;
and the discrete control OT with $s = 5$ segments. For Transfer (IA),
a reference trajectory (RT) was also computed: this is a nonoptimal
discrete-control trajectory with $s = 5$ segments, obtained by means
of the restoration algorithm, starting from a nominal trajectory
supplied in Ref. 5. Thus, a total of 11 trajectories were computed,
ten optimal trajectories and one reference trajectory. The
numerical results are shown in Tables 1-2 and Figs. 1-2.

Table 1 shows the values of the characteristic velocity ΔV
and the flight time τ for all the trajectories computed. For
Transfer (IA), the reference trajectory requires $\Delta V = 98.0$ m/sec
and a flight time $\tau = 488$ sec; also for Transfer (IA), the
optimal trajectories require $\Delta V = 81.9$ m/sec and a flight time
$\tau = 796$ sec. For Transfer (DA), the optimal trajectories require
$\Delta V = 72.0$ m/sec and a flight time $\tau = 820$ sec. To sum up,
the optimal trajectories are considerably more efficient propulsively
than the reference trajectory and they are characterized by a
longer flight time.

An interesting result of the analysis is that, for each transfer, the optimal continuous-control trajectory and the optimal discrete-control trajectories coalesce into a single trajectory: a two-subarc trajectory, with the bank angle constant in each subarc (bang-bang control). Specifically, the bank angle is near 180 deg in the atmospheric entry phase (positive lift projection phase) and is near 0 deg in the atmospheric exit phase (negative lift projection phase). This is true for both Transfer (IA) and Transfer (DA). See Figs. 1-2.

In the light of the above statement, we now focus attention on only three trajectories: for Transfer (IA), the reference trajectory and the two-subarc optimal trajectory; for Transfer (DA), the two-subarc optimal trajectory. For these trajectories, Table 2 shows the values of the following quantities: the characteristic velocity; the flight time; the minimum altitude; the peak dynamic pressure; the peak heating rate; the peak change of the orbital inclination; the peak change of the longitude of the ascending node; and the peak value of the wedge angle.

Table 2 illustrates clearly the advantages of the OTs with respect to the reference trajectory. Concerning the longitudinal motion, by comparison with the RT, the OTs are characterized by smaller ΔV and also by smaller values of the peak dynamic pressure and the peak heating rate; this is due to the fact that the minimum altitude of the OTs is about 3 km higher than the minimum altitude of the RT. Concerning the lateral motion, by comparison with the RT, the OTs exhibit smaller values of the peak change of the orbital inclination and the peak change

of the longitude of the ascending node; hence, the peak wedge

angle of the OTs is smaller than the corresponding quantity for

the RT.   Indeed, it is suprising that $\max|\Delta i|$ and $\max|\Delta\Omega|$ are

nearly zero for the OTs; hence, $\max(\eta)$ is nearly zero for the OTs.

This means that, for efficient flight, the motion of the spacecraft

must be nearly planar in an inertial space; in other words, one

must avoid energy dissipation associated with the lateral motion.

More details on the trajectories computed can be found in

Figs. 1 and 2.   Figure 1 refers to Transfer (IA), and Fig. 2 refers

to Transfer (DA).   These figures include the time histories of

the following quantities: the bank angle (Figs. 1A and 2A); the

altitude (Figs. 1B and 2B); the relative velocity (Figs. 1C and 2C);

the relative path inclination (Figs. 1D and 2D); the dynamic

pressure (Figs. 1E and 2E); the heating rate (Figs. 1F and 2F);

and the wedge angle (Figs. 1G and 2G).

Remark. With reference to the two-subarc OTs of Transfer (IA)

and Transfer (DA), we observe that the value of the bank angle

is μ = 176.7 deg for the atmospheric entry phase and μ = 5.5 deg

for the atmospheric exit phase.   Let L denote the lift, and let

$$L_p = L\cos\mu, \qquad L_q = L\sin\mu \qquad\qquad (12)$$

denote the vertical component and the lateral component of the

lift.   Let C_L, C_{Lp}, C_{Lq} denote the associated lift coefficients,

and observe that

$$C_{Lp} = C_L \cos\mu, \qquad C_{Lq} = C_L \sin\mu. \qquad (13)$$

We recall that the AFE spacecraft flies at constant angle of attack $\alpha = 17$ deg, corresponding to $C_L = -0.3707$ and $C_D = 1.315$. With this understanding, we see that, for the atmospheric entry phase,

$$C_{Lp} = -0.998 \, C_L, \qquad C_{Lq} = 0.058 C_L; \qquad (14)$$

and we see that, for the atmospheric exit phase,

$$C_{Lp} = 0.995 \, C_L, \qquad C_{Lq} = 0.096 \, C_L. \qquad (15)$$

Therefore, the following comments arise:

(i)   in the atmospheric entry phase, the vertical component of the lift is directed upward and its modulus is only 2/1000 smaller than the lift modulus; this causes the path inclination to increase gradually from the entry negative value to nearly zero value;

(ii) in the atmospheric exit phase, the vertical component of the lift is directed downward and its modulus is only 5/1000 smaller than the lift modulus; this offsets the centrifugal force effects due to the curvature of the Earth, so as to ensure exit conditions compatible with the desired apogee requirement;

(iii) the lateral component of the lift during the atmospheric entry phase and the lateral component of the lift during the atmospheric exit phase have the same sign and the same order of magnitude; their modulus is 5.8% of the lift modulus in the atmospheric entry phase and 9.6% of the lift modulus in the atmospheric

exit phase; these lateral lift components are directed in such a
way that they nearly offset the effects due to the Earth's
rotation, so as to ensure exit conditions compatible with the
desired wedge angle requirement.

7.   Guidance Implications

The results of Section 6 provide a foundation for developing

a more efficient guidance scheme for the AFE spacecraft. For

information concerning the existing guidance scheme, see Refs. 5

and 21.

First, we recall the basic idea of the existing guidance

scheme. For the AFE spacecraft, the angle of attack varies from

7 to 27 deg, and the lift coefficient varies from -0.47 to -0.21.

Therefore, if the AFE spacecraft were to be controlled via only

the angle of attack, the lift coefficient range would be $|\Delta C_L| = 0.26$.

To offset the above difficulty, the existing guidance scheme

employs a constant angle of attack α = 17 deg, corresponding to

C_L = -0.37, coupled with a variable angle of bank.

Let L_p = Lcosμ denote the projection of the lift vector in

the vertical direction; let C_{Lp} = $C_L$cosμ denote the projected

lift coefficient. Because C_L is constant and cosμ varies from

-1 to +1, the projected lift coefficient range is $|\Delta C_{Lp}| = 0.74$.

This is nearly triple the lift coefficient range $|\Delta C_L| = 0.26$.

To sum up, for the AFE spacecraft, the existing guidance

scheme employs constant angle of attack and variable angle of

bank in order to achieve the following goals:for the longitudinal

motion, to dissipate excess velocity so that the spacecraft,

upon exiting the atmosphere, can ascend to a specified apogee;

and for the lateral motion, to keep the instantaneous orbital plane

close to the initial orbital plane, hence to keep the wedge

angle close to zero.   These goals are achieved as follows: for the longitudinal motion, one controls the modulus of the bank angle; for the lateral motion, one controls the sign of the bank angle;   thus, whenever the wedge angle exceeds a specified bound, the sign of the bank angle is reversed.

Unquestionably, the existing guidance scheme has obvious merits: (a) simplicity; and (b) the fact that the projected lift coefficient range is three times the lift coefficient range. However, there are weaknesses associated with the control of the lateral motion:

(A)   There is no equilibrium point for the control of the lateral motion.   When $\eta = 0$, it would be desirable to have $\dot{\eta} = 0$, so that the wedge angle continues to be zero.   However, μ is determined from the requirement of longitudinal motion control; hence, generally speaking, $\dot{\eta} \neq 0$ when $\eta = 0$.   This means that the system is not stable around $\eta = 0$.

(B)   There is a bank angle error due to noninstantaneous switches.   The implementation of the existing guidance scheme ideally requires instantaneous switches in $\text{sign}(\mu)$, so as to keep $\cos\mu$ unchanged.   In practice, this is not possible, since $|\dot{\mu}| \leq 20$ deg/sec. For example, a switch from $\mu = +170$ to $\mu = -170$ deg requires $\Delta t = 17$ sec.   If the correct μ-values are $\mu = +170$ and $\mu = -170$ deg, this means that, during the time interval $\Delta t = 17$ sec, there is an error in the value of μ which is required for the control of the longitudinal motion.

(C)   There is a contradiction between accuracy and stability. For accurate control of the lateral motion, the wedge angle tolerance should be small. On the other hand, if the wedge angle tolerance is small, the number of switches in $\text{sign}(\mu)$ increases; therefore, the system stability becomes worse.

To offset the above difficulties, consideration should be given to developing a new guidance scheme, based on the properties of the optimal trajectories. The basic ideas of the new guidance scheme are: to control both the angle of attack (near 17 deg) and the angle of bank; and to utilize a single switch of the bank angle, consistently with the optimal trajectory properties, so as to have $L_p > 0$ in the entry phase and $L_p < 0$ in the exit phase; here, L_p is the projected lift. The new guidance scheme retains the basic advantage of the existing guidance scheme, in that the projected lift coefficient range is three times the lift coefficient range. In addition, it has the following advantages:

(A)   There is an equilibrium point for the control of the lateral motion, due to the fact that both the angle of attack and the angle of bank are being varied. Hence, when $\eta = 0$, it is possible to have $\dot\eta = 0$, which means that the system is stable around $\eta = 0$.

(B)   There is less bank angle error due to noninstantaneous switches. For the existing guidance scheme, the effects due to the noninstantaneous switch from $+\mu$ to $-\mu$ can be serious, since there are multiple switches and they occur randomly. For the new

guidance scheme, the effects due to the noninstantaneous switch from $+\mu$ to $-\mu$ are less serious, owing to the fact that there is only one switch, which occurs whenever a preselected velocity is achieved.

(C) There is improved accuracy and stability in the control of the lateral motion. This is because the lateral motion is no longer controlled by the sign of the bank angle, but by the values of both the bank angle and the angle of attack.

(D) The new guidance scheme is based on the properties of the optimal trajectories. Hence, it preserves the good properties of the optimal trajectories concerning the characteristic velocity, the peak dynamic pressure, the peak heating rate, and the peak wedge angle.

(E) The new guidance scheme uses the same hardware (AFE configuration, measurements, sensors, and reaction control system) as the existing guidance scheme. The only difference is in the software (computer code). Therefore, if acceptable, a change from the existing guidance scheme to the new guidance scheme would be of limited cost.

8. Conclusions

In this report, the trajectories of an AFE spacecraft are
analyzed in a 3D-space, employing the full system of 6 ODEs
describing the atmospheric pass. It is assumed that the angle
of attack is constant and that the spacecraft is controlled via
only the angle of bank. It is also assumed that the atmospheric
entry conditions are given and that the atmospheric exit conditions
are adjusted in such a way that the following conditions are
satisfied: (a) the atmospheric velocity depletion is such that,
after exiting, the AFE spacecraft first ascends to a specified
apogee and then descends to a specified perigee; and (b) the
exit orbital plane is identical with the entry orbital plane.

Under the above conditions, optimal trajectories are
determined by minimizing the total characteristic velocity, hence
the propellant consumption required for orbital transfer. The
resulting optimization problems are solved by means of the sequential
gradient-restoration algorithm.

Two possible transfers are considered: (IA) indirect ascent
to a 178 NM perigee via a 197 NM apogee; and (DA) direct ascent
to a 178 NM apogee. For both transfers, two cases are investigated:
(i) the bank angle is continuously variable; and (ii) the trajectory
is divided into segments along which the bank angle is constant.
For case (ii), the following subcases are studied: two segments,
three segments, four segments, and five segments; because the time
duration of each segment is optimized, the above subcases involve

four, six, eight, and ten parameters, respectively. For comparison

purposes and only for Transfer (IA), a reference trajectory is

also considered: this is a five-segment trajectory, close to the

nominal trajectory given in Ref. 5.

From the extensive numerical computations, the following

conclusions arise:

(i)   The optimal trajectories are two-subarc trajectories,

with the bank angle constant in each subarc; hence, the control

is bang-bang.

(ii)   In the atmospheric entry phase, the bank angle is

near 180 deg,yielding a positive projected lift, which in turn

causes the path inclination to increase gradually from the entry

negative value to nearly zero value.

(iii) In the atmospheric exit phase, the bank angle is near

0 deg,   yielding a negative projected lift, which offsets the

centrifugal force effects due to the curvature of the Earth, so

as to ensure exit conditions compatible with the desired apogee

requirement.

(iv)   The lateral component of the lift during the atmospheric

entry phase and the lateral component of the lift during the

atmospheric exit phase have the same sign and the same order of

magnitude; they are directed in such a way that they nearly offset

the effects due to the Earth's rotation. In this way, the

instantaneous orbital plane is almost identical with the initial

orbital plane, meaning that the wedge angle is nearly zero during

the atmospheric pass.   This means that, for efficient flight, the
motion of the AFE spacecraft is nearly planar in an inertial space;
in other words, one must avoid energy dissipation associated with
the lateral motion.

(v)   Comparison of the optimal trajectories and the reference
trajectory shows that the OTs are superior to the RT in terms
of the main quantities of interest, namely, the characteristic
velocity, the peak dynamic pressure, the peak heating rate, and
the peak wedge angle.   In particular, for Transfer (IA), the
characteristic velocity is ΔV = 98.0 m/sec for the RT and
ΔV = 81.9 m/sec for the OT.   For Transfer (DA), the characteristic
velocity of the OT is 72.0 m/sec.

(vi)   The results on optimal trajectories have important
guidance implications.   They suggest the idea of developing a
new guidance scheme based on the following precepts: to control
both the angle of attack (near 17 deg) and the angle of bank;
and to utilize a single switch of the bank angle, so as to have
L_p > 0 in the entry phase and L_p < 0 in the exit phase. This
new guidance system is promising, and it appears to be an improvement of
the existing guidance scheme in the control of the lateral motion
of the AFE spacecraft.

References

1.   MIELE, A., ZHAO, Z. G., and LEE, W. Y., <u>Optimal Trajectories for the Aeroassisted Flight Experiment, Part 1, Equations of Motion in an Earth-Fixed System</u>, Rice University, Aero-Astronautics Report No. 238, 1989.

2.   MIELE, A., ZHAO, Z. G., and LEE, W. Y., <u>Optimal Trajectories for the Aeroassisted Flight Experiment, Part 2, Equations of Motion in an Inertial System</u>, Rice University, Aero-Astronautics Report No. 239, 1989.

3.   MIELE, A., WANG, T., LEE, W. Y., and ZHAO, Z. G., <u>Optimal Trajectories for the Aeroassisted Flight Experiment, Part 3, Formulation, Results, and Analysis</u>, Rice University, Aero-Astronautics Report No. 242, 1989.

4.   MIELE, A., WANG, T., LEE, W. Y., WANG, H., and WU, G. D., <u>Optimal Trajectories for the Aeroassisted Flight Experiment, Part 4, Data, Tables, and Graphs</u>, Rice University, Aero-Astronautics Report No. 243, 1989.

5.   ANONYMOUS, N. N., <u>Aeroassisted Flight Experiment: Preliminary Design Document</u>, NASA Marshall Space Flight Center, 1986.

6.   MIELE, A., PRITCHARD, R. E., and DAMOULAKIS, J. N., <u>Sequential Gradient-Restoration Algorithm for Optimal Control Problems</u>, Journal of Optimization Theory and Applications, Vol. 5, No. 4, pp. 235-282, 1970.

7.   MIELE, A., DAMOULAKIS, J. N., CLOUTIER, J. R.,and TIETZE, J. L.,
      Sequential Gradient-Restoration Algorithm for Optimal
      Control Problems with Nondifferential Constraints, Journal
      of Optimization Theory and Applications, Vol. 12, No. 2,
      pp. 218-255, 1974.

8.   MIELE, A.,   Recent Advances in Gradient Algorithms for
      Optimal Control Problems, Journal of Optimization Theory
      and Applications, Vol. 17, Nos. 5-6, pp. 361-430, 1975.

9.   MIELE, A., Gradient Algorithms for the Optimization of
      Dynamic Systems, Control and Dynamic Systems, Advances in
      Theory and Application, Edited by C. T. Leondes, Academic
      Press, New York, New York, Vol. 16, pp. 1-52, 1980.

10.   MIELE, A., and WANG, T., Primal-Dual Properties of Sequential
      Gradient-Restoration Algorithms for Optimal Control Problems,
      Part 1, Basic Problem, Integral Methods in Science and
      Engineering, Edited by F. R. Payne et al, Hemisphere Publishing
      Corporation, Washington, DC, pp. 577-607, 1986.

11.   MIELE, A., and WANG, T., Primal-Dual Properties of Sequential
      Gradient-Restoration Algorithms for Optimal Control Problems,
      Part 2, General Problem, Journal of Mathematical Analysis
      and Applications, Vol. 119, Nos. 1-2, pp. 21-54, 1986.

12.   MIELE, A., WANG, T., and BASAPUR, V. K., Primal and Dual
      Formulations of Sequential Gradient-Restoration Algorithms
      for Trajectory Optimization Problems, Acta Astronautica,
      Vol. 13, No. 8, pp. 491-505, 1986.

13. MIELE, A., and VENKATARAMAN, P., Optimal Trajectories for
     Aeroassisted Orbital Transfer, Acta Astronautica, Vol.11,
     Nos. 7-8, pp. 423-433, 1984.

14. MIELE, A., and BASAPUR, V. K., Approximate Solutions to
     Minimax Optimal Control Problems for Aeroassisted Orbital
     Transfer, Acta Astronautica, Vol. 12, No. 10, pp. 809-818, 1985.

15. MIELE, A., BASAPUR, V. K., and MEASE, K. D., Nearly-Grazing
     Optimal Trajectories for Aeroassisted Orbital Transfer,
     Journal of the Astronautical Sciences, Vol. 34, No. 1, pp.
     3-18, 1986.

16. MIELE, A., BASAPUR, V. K., and LEE, W. Y., Optimal Trajectories
     for Aeroassisted, Coplanar Orbital Transfer, Journal of
     Optimization Theory and Applications, Vol. 52, No. 1, pp. 1-24,
     1987.

17. MIELE, A., BASAPUR, V. K., and LEE, W. Y., Optimal Trajectories
     for Aeroassisted, Noncoplanar Orbital Transfer, Acta Astronautica,
     Vol. 15, Nos. 6-7, pp. 399-411, 1987.

18. MIELE, A., LEE, W. Y., and MEASE, K. D., Optimal Trajectories
     for LEO-to-LEO Aeroassisted Orbital Transfer, Acta Astronautica,
     Vol. 18, Nos. 1-12, pp. 99-122, 1988.

19. MIELE, A., LEE, W. Y., and MEASE, K. D., Nearly-Grazing Optimal
     Trajectories for Aeroassisted, Noncoplanar Orbital Transfer,
     Journal of the Astronautical Sciences, Vol. 36, Nos. 1-2,
     pp. 139-157, 1988.

20. NOAA, NASA, and USAF, <u>US Standard Atmosphere, 1976</u>, US
     Government Printing Office, Washington, DC, 1976.

21. GAMBLE, J. D., CERIMELE, C. J., MOORE, T. E., and HIGGINS, J.,
     <u>Atmospheric Guidance Concepts for an Aeroassist Flight
     Experiment</u>, Journal of the Astronautical Sciences, Vol. 36,
     Nos. 1-2, pp. 45-71, 1988.

List of Tables

List of Figures

Table 1. Characteristic velocity and flight time.

Trajectory	Control	s	ΔV (m/sec)	τ (sec)
IART	Discrete	5	97.97	487.6
IAOT	Continuous	∞	81.86	795.3
IAOT	Discrete	2	81.86	795.7
IAOT	Discrete	3	81.86	795.7
IAOT	Discrete	4	81.86	795.8
IAOT	Discrete	5	81.84	796.2
DAOT	Continuous	∞	72.05	817.6
DAOT	Discrete	2	72.03	819.5
DAOT	Discrete	3	72.03	819.6
DAOT	Discrete	4	72.03	819.6
DAOT	Discrete	5	72.01	819.9

IA = indirect ascent,   DA = direct ascent,

OT = optimal trajectory,   RT = reference trajectory,

s = number of segments.

Table 2. Comparison of AFE trajectories.

Quantity	IART s = 5	IAOT s = 2	DAOT s = 2	Units
ΔV	97.97	81.86	72.03	m/sec
τ	487.6	795.7	819.5	sec
min(h)	74.6	77.5	77.5	km
max(DP)	1629	1174	1174	N/m^2
max(HR)	158	148	148	W/cm^2
$\max\|\Delta i\|$	1.08	0.01	0.01	deg
$\max\|\Delta\Omega\|$	0.32	0.00	0.00	deg
$\max(\eta)$	1.08	0.01	0.01	deg

IA = indirect ascent,   DA = direct ascent,

OT = optimal trajectory,   RT = reference trajectory,

s = number of segments.
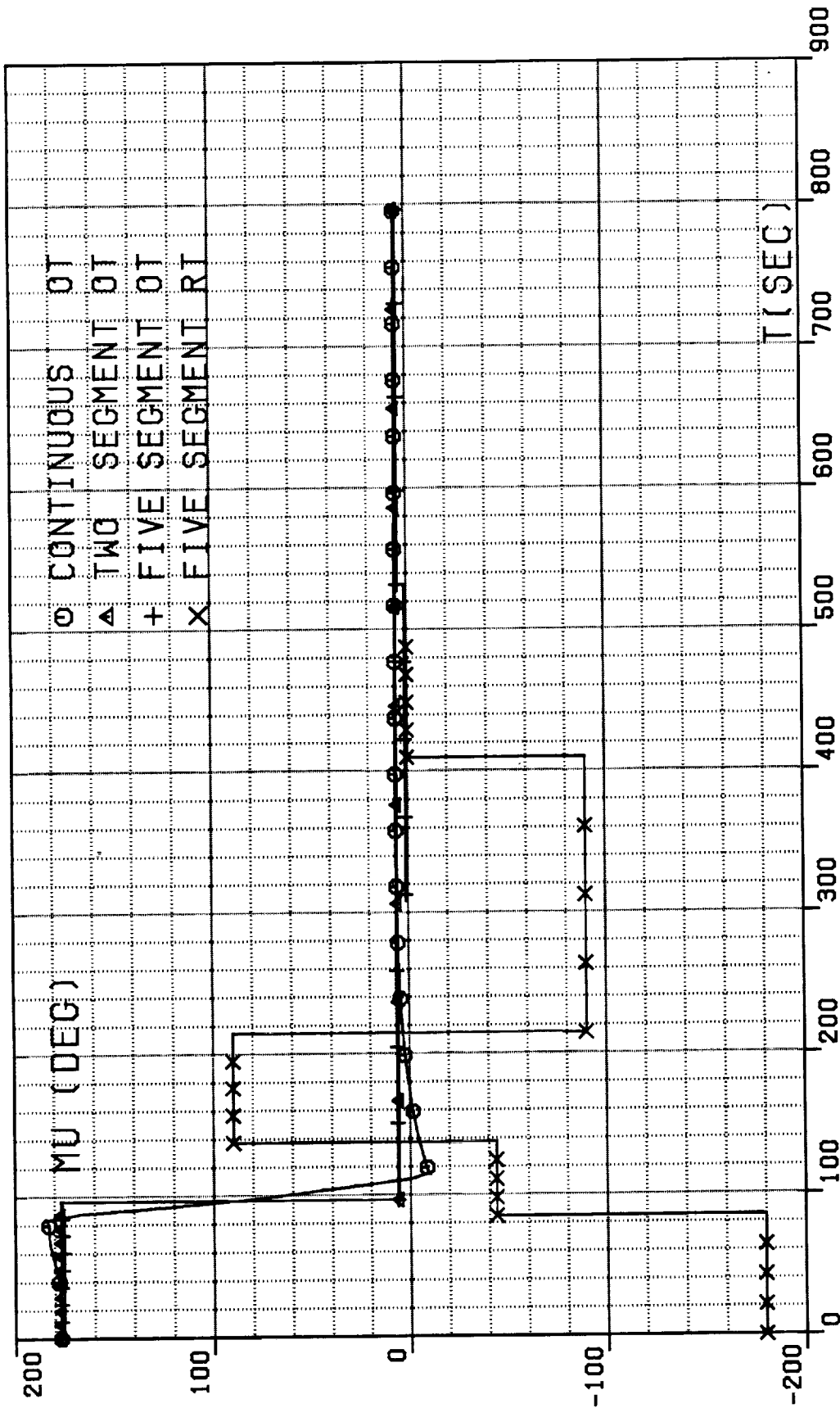
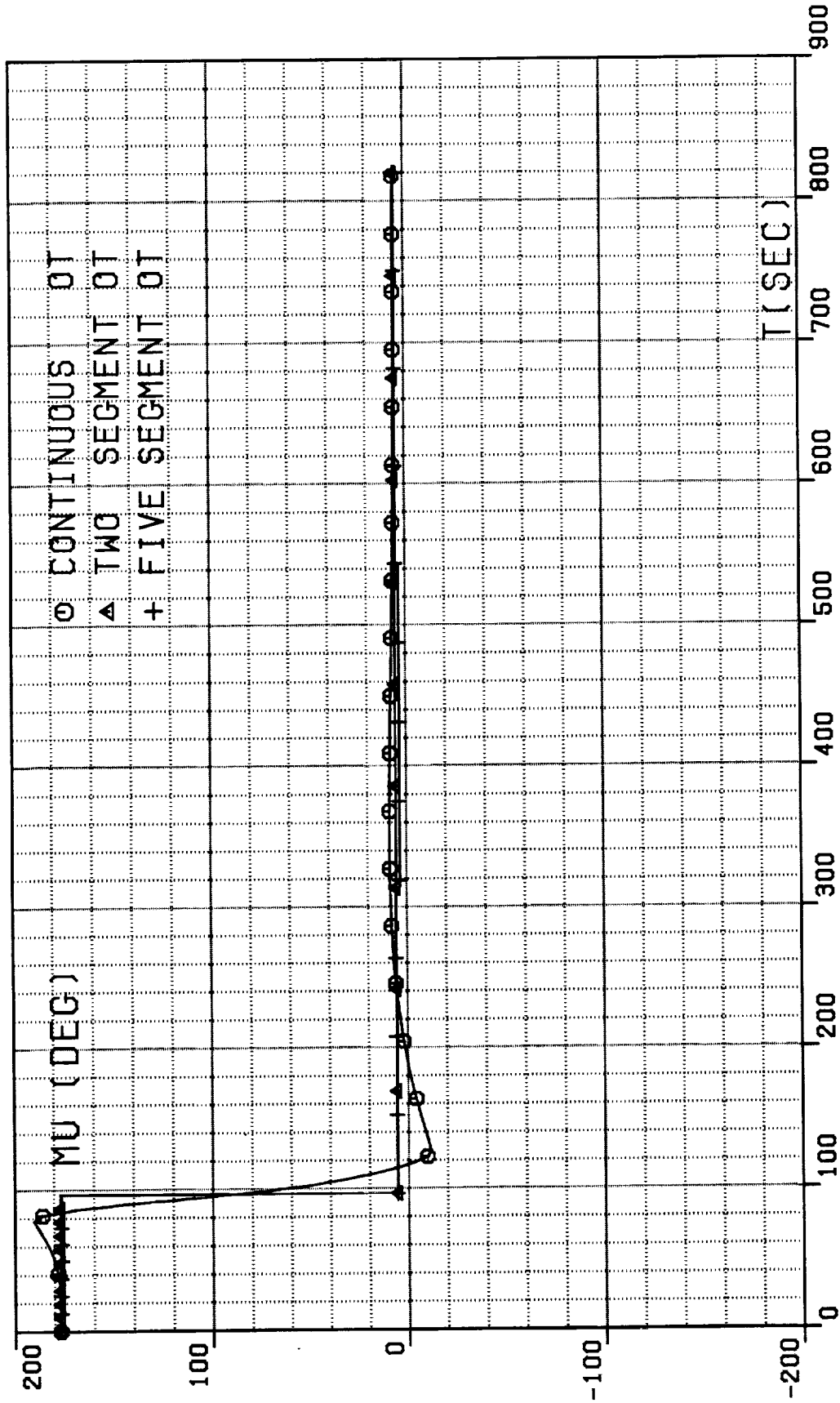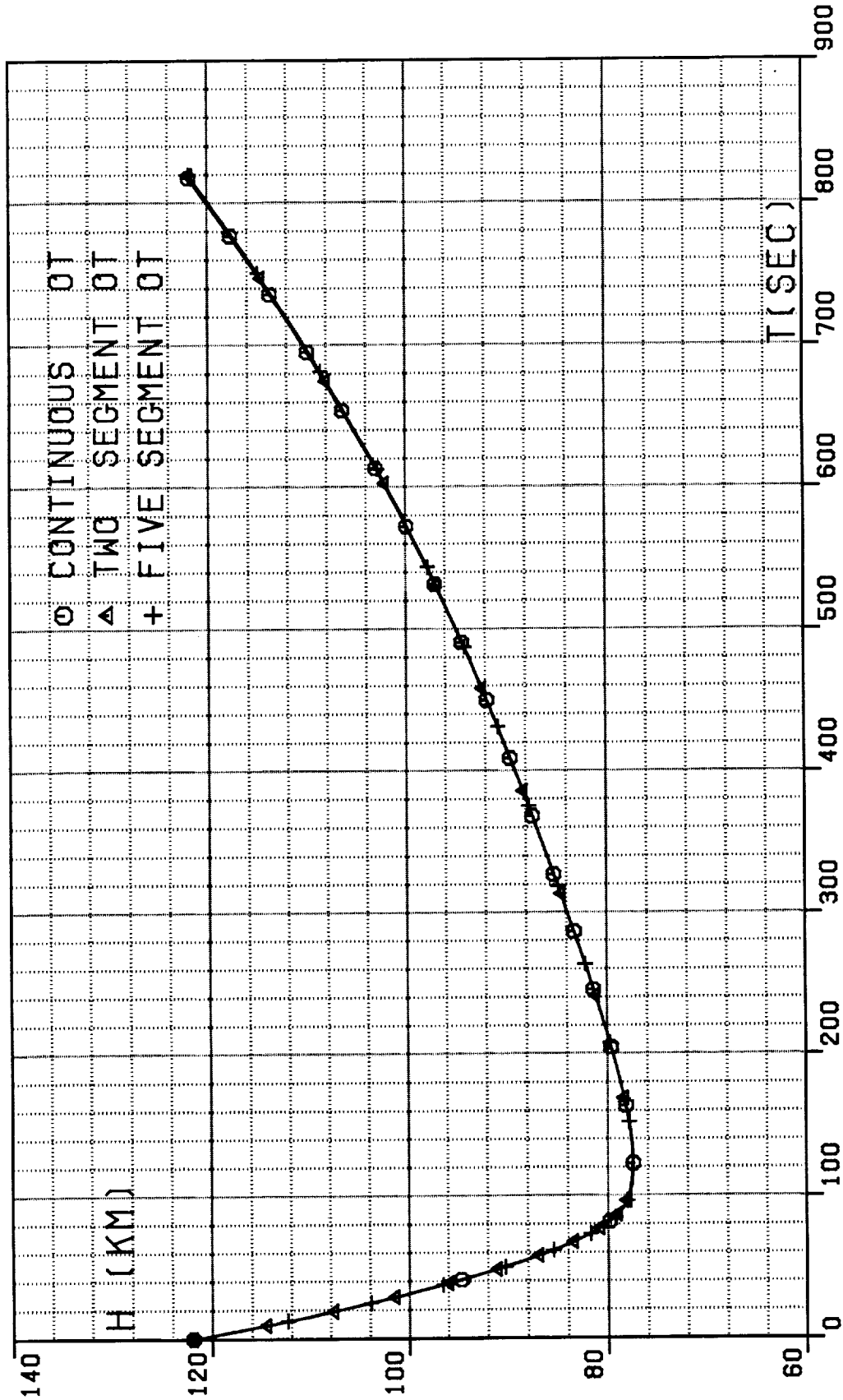FIG. 1A. COMPARISON OF AFE TRAJECTORIES, TRANSFER (IA), BANK ANGLE.
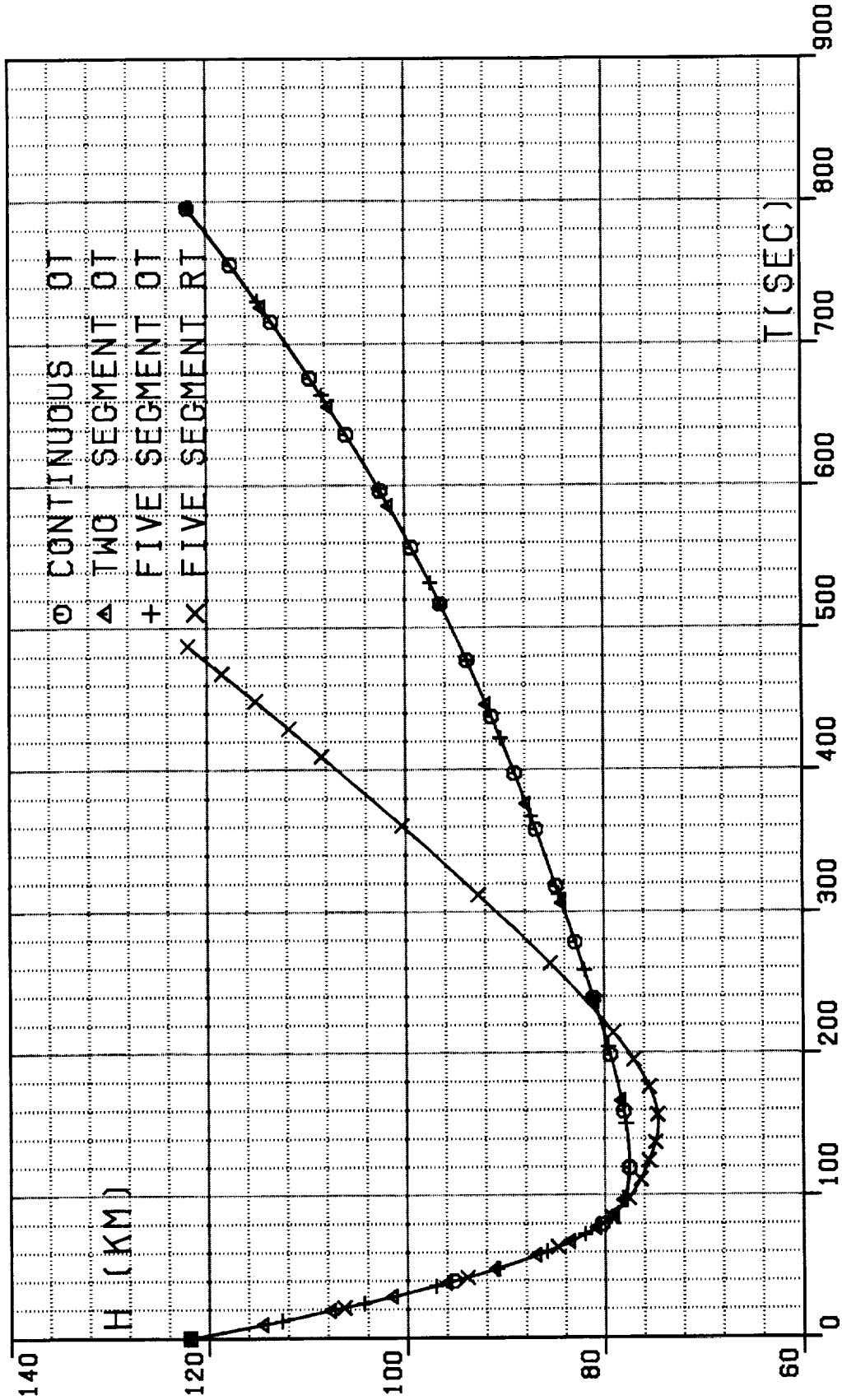
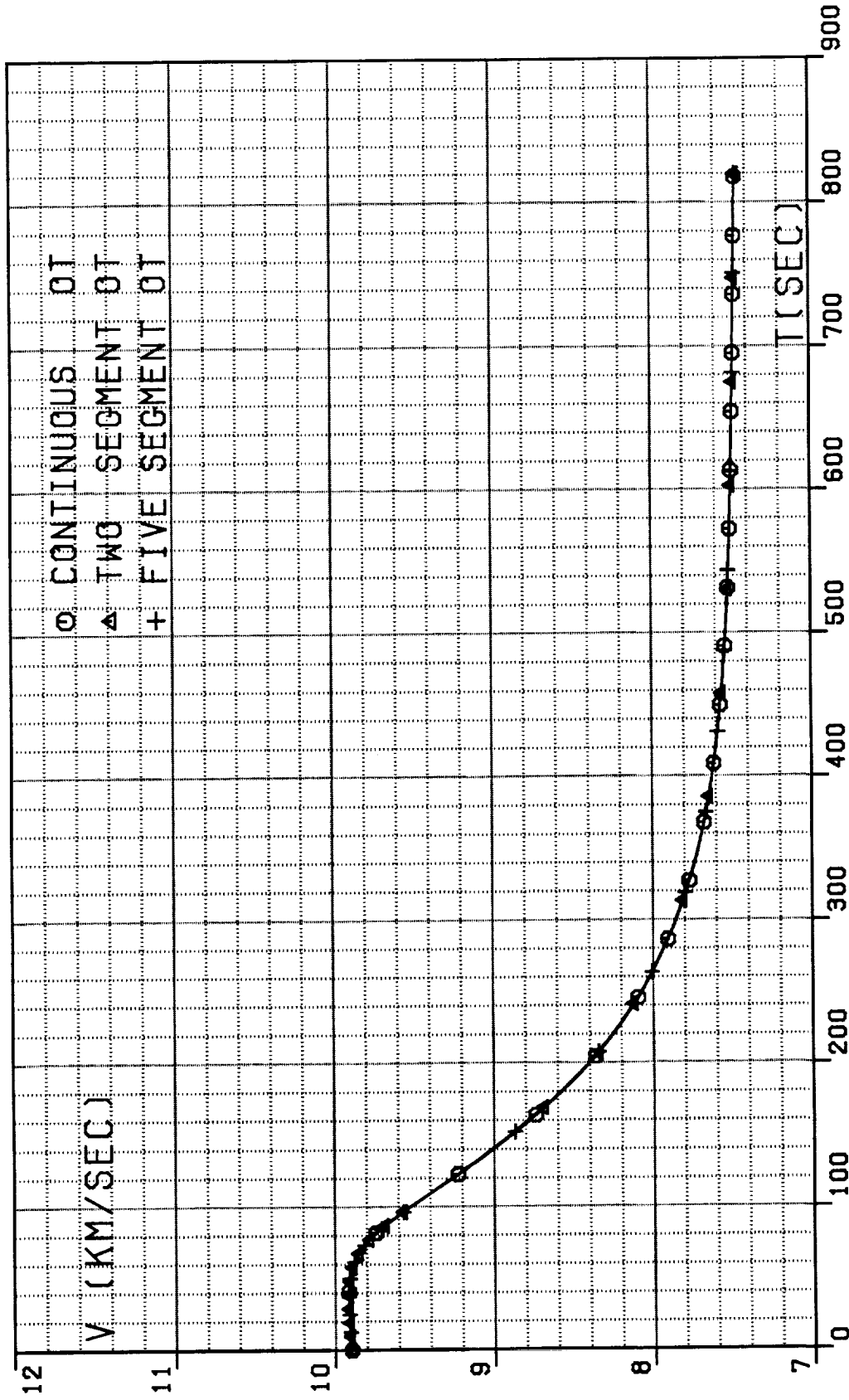FIG.1B. COMPARISON OF AFE TRAJECTORIES, TRANSFER (IA), ALTITUDE.
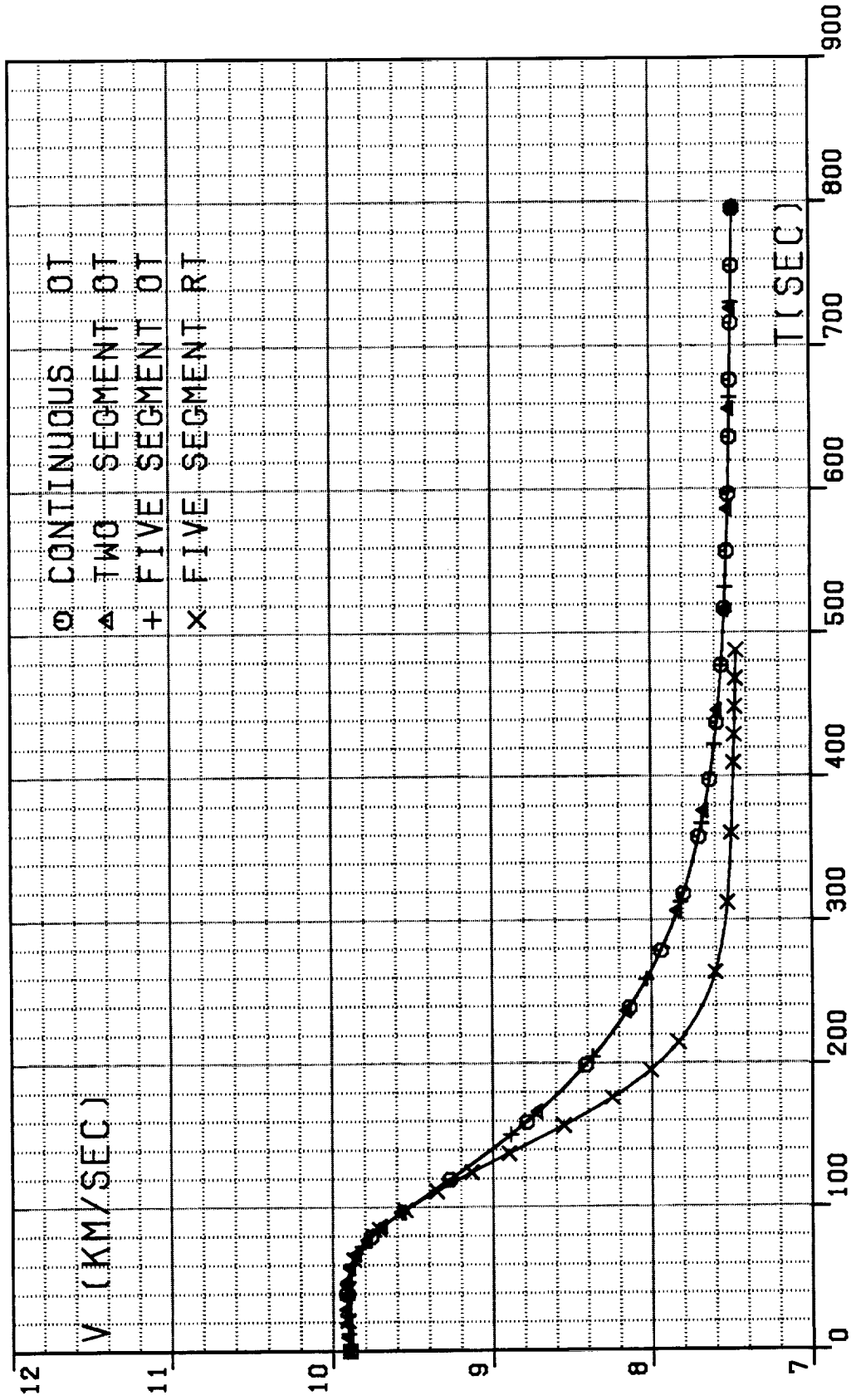
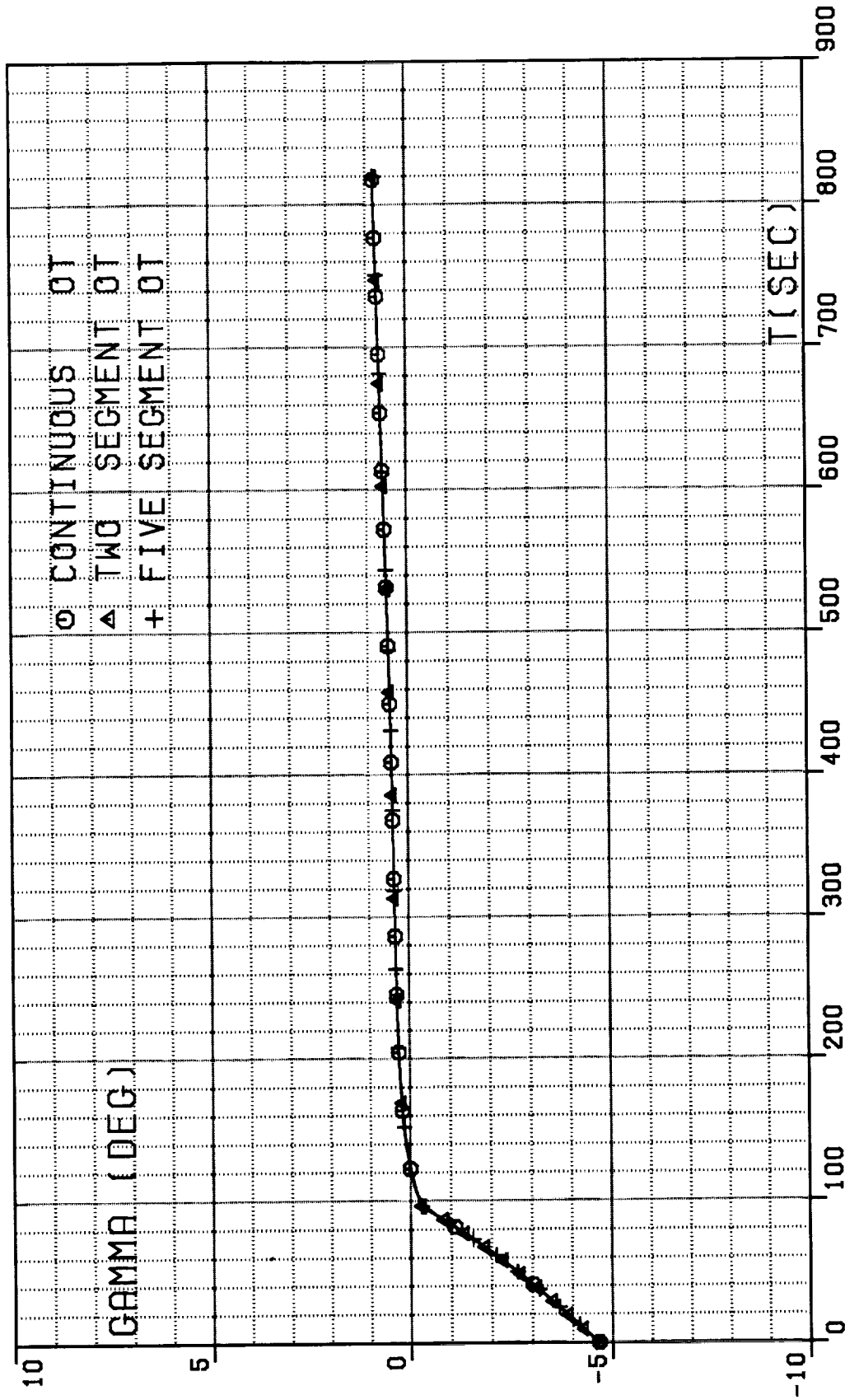FIG.1C. COMPARISON OF AFE TRAJECTORIES,
TRANSFER (IA), RELATIVE VELOCITY.
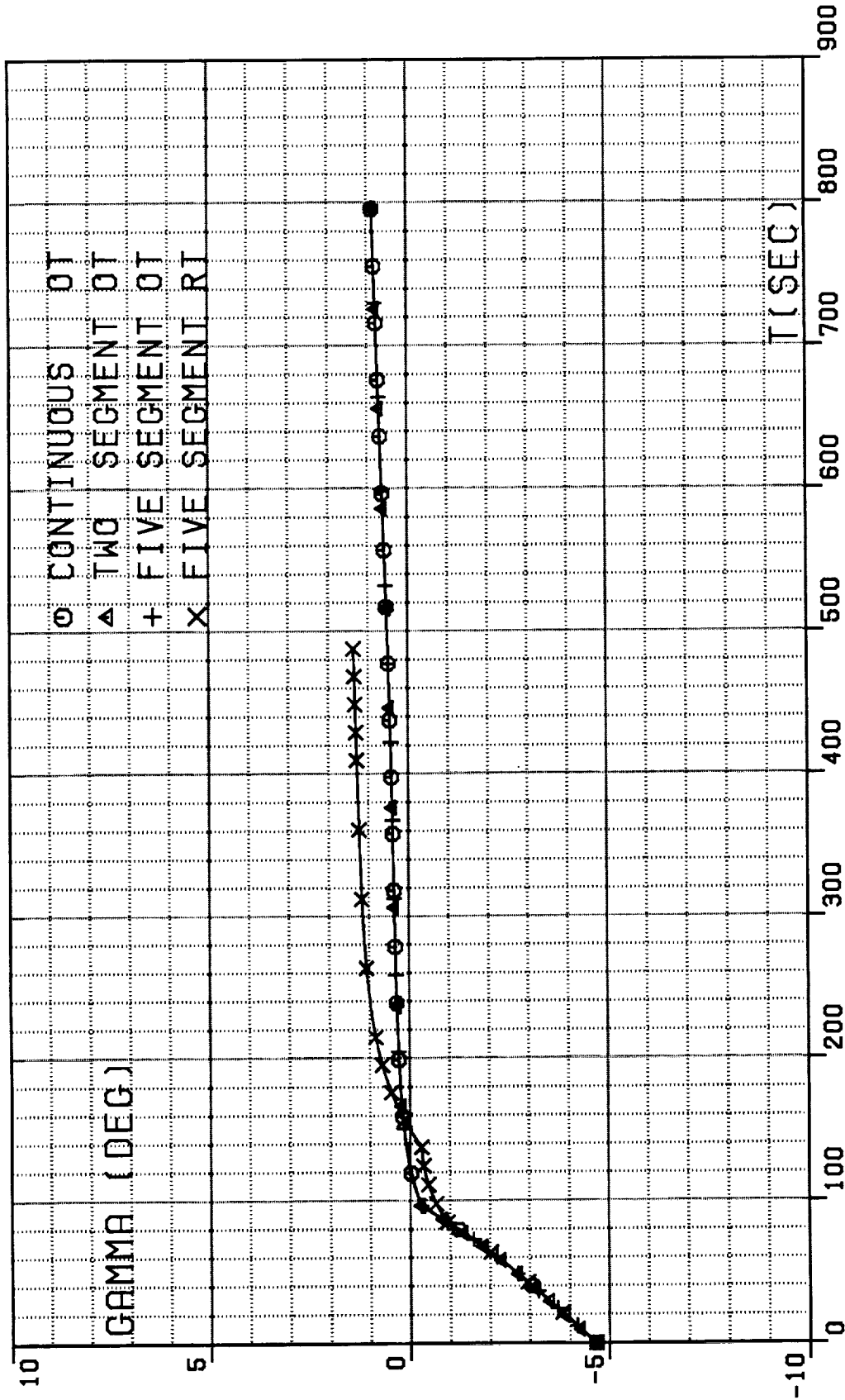
FIG.1D. COMPARISON OF AFE TRAJECTORIES,
TRANSFER (IA), RELATIVE PATH INCLINATION.
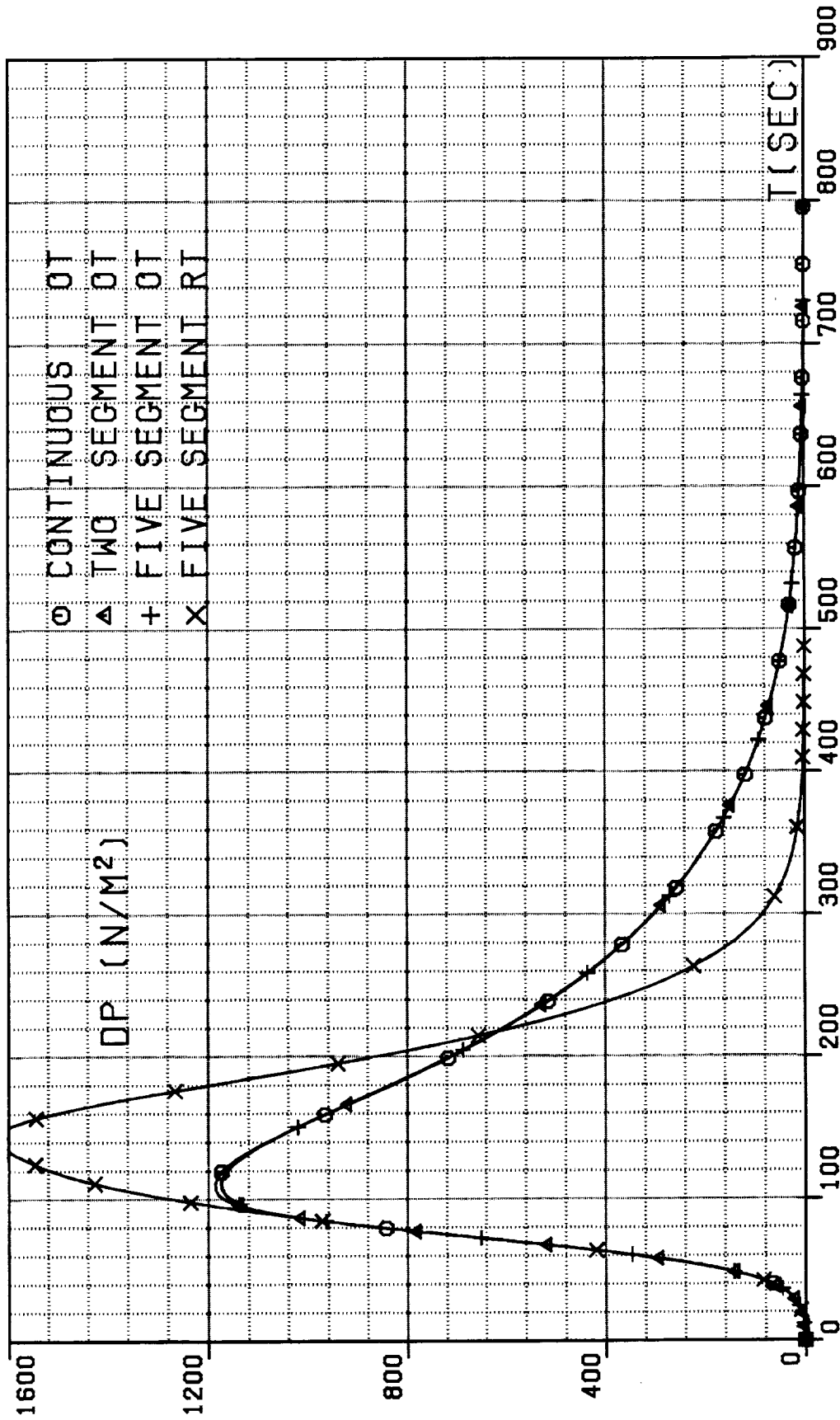
FIG.1E. COMPARISON OF AFE TRAJECTORIES,
TRANSFER (IA), DYNAMIC PRESSURE.
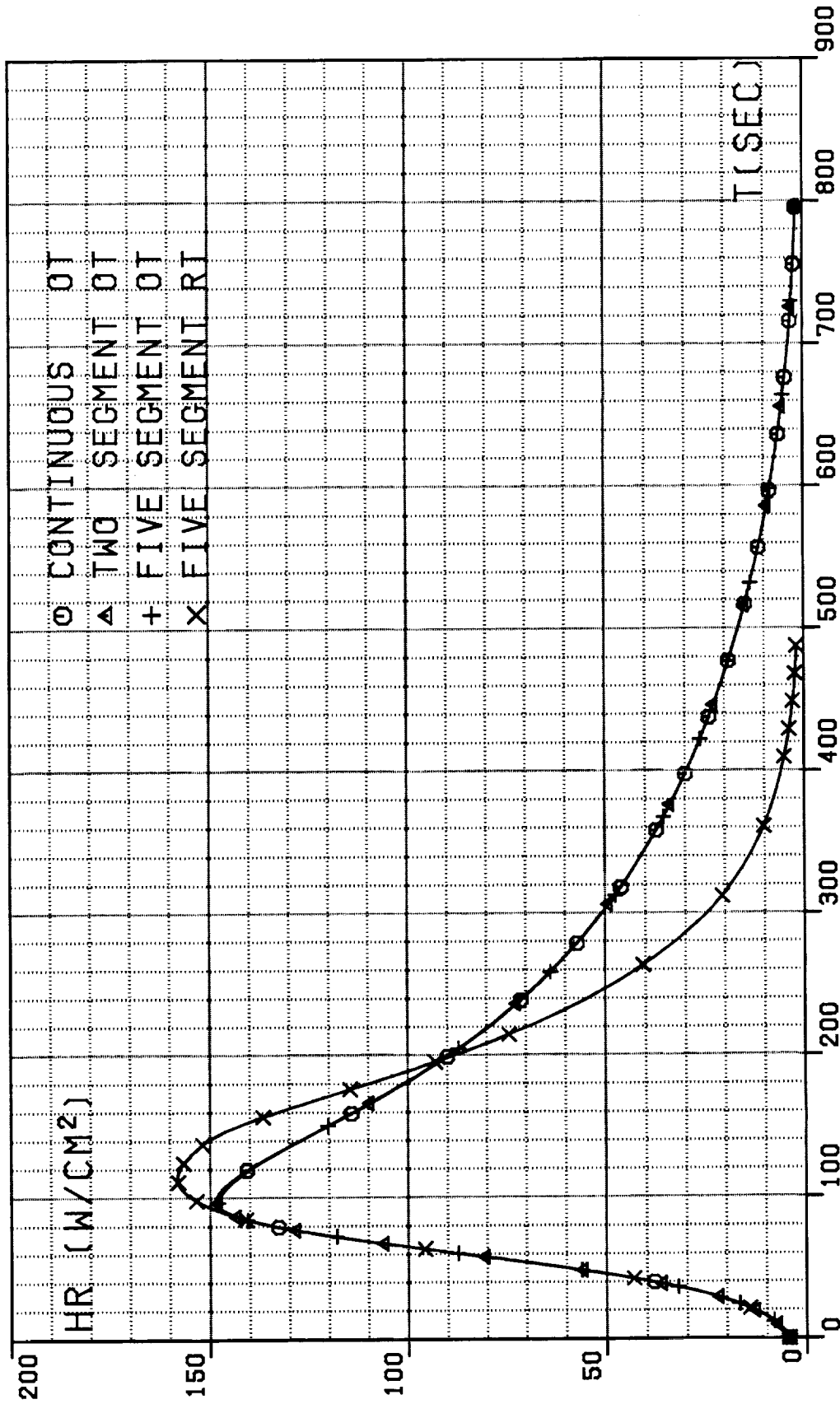
FIG.1F. COMPARISON OF AFE TRAJECTORIES, TRANSFER (IA), HEATING RATE.
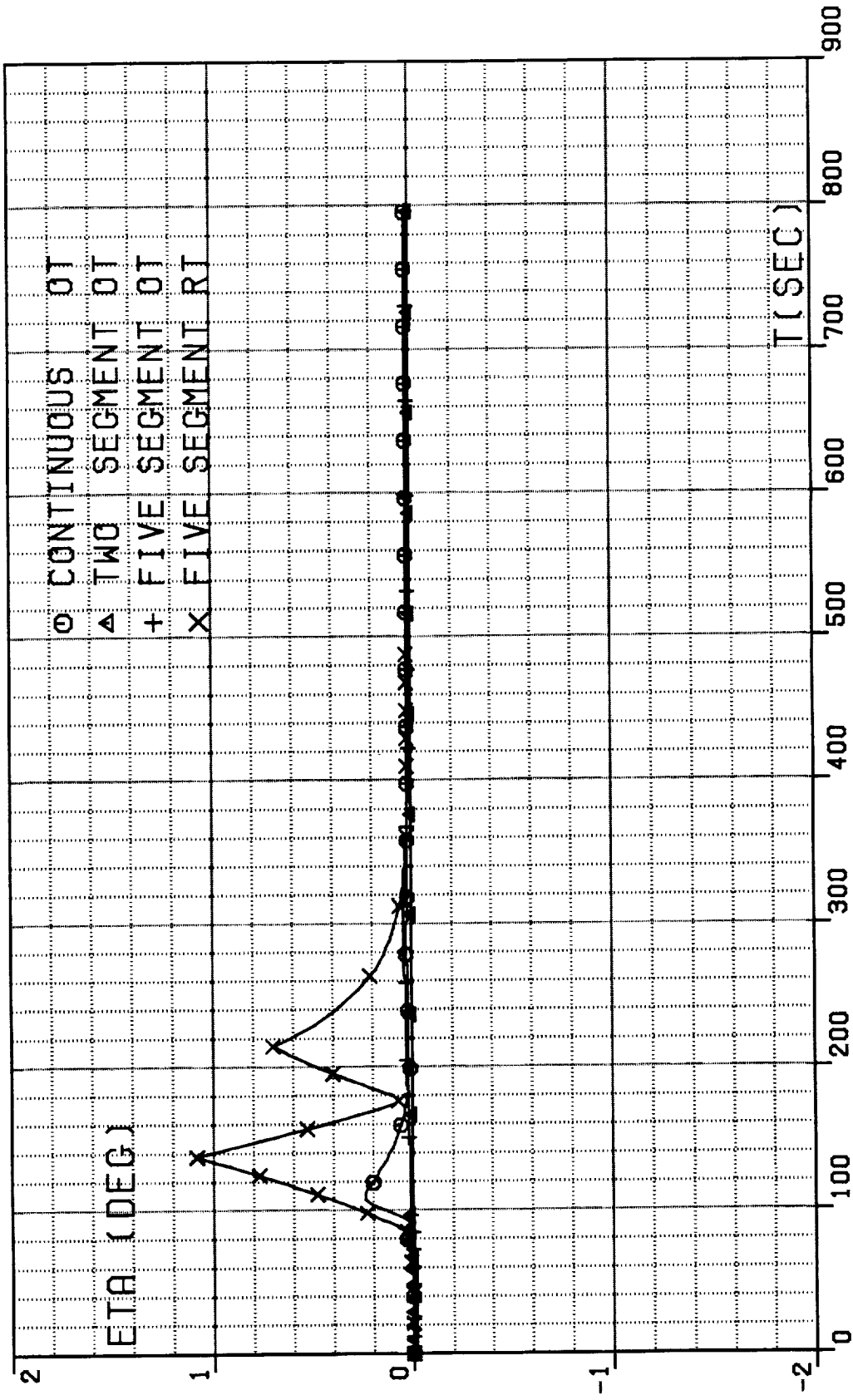
FIG.1G. COMPARISON OF AFE TRAJECTORIES, TRANSFER (IA), WEDGE ANGLE.

FIG.2A. COMPARISON OF AFE TRAJECTORIES, TRANSFER (DA), BANK ANGLE.

FIG.2B. COMPARISON OF AFE TRAJECTORIES,
TRANSFER (DA), ALTITUDE.

FIG.2C. COMPARISON OF AFE TRAJECTORIES,
TRANSFER (DA), RELATIVE VELOCITY.

FIG. 2D. COMPARISON OF AFE TRAJECTORIES, TRANSFER (DA), RELATIVE PATH INCLINATION.
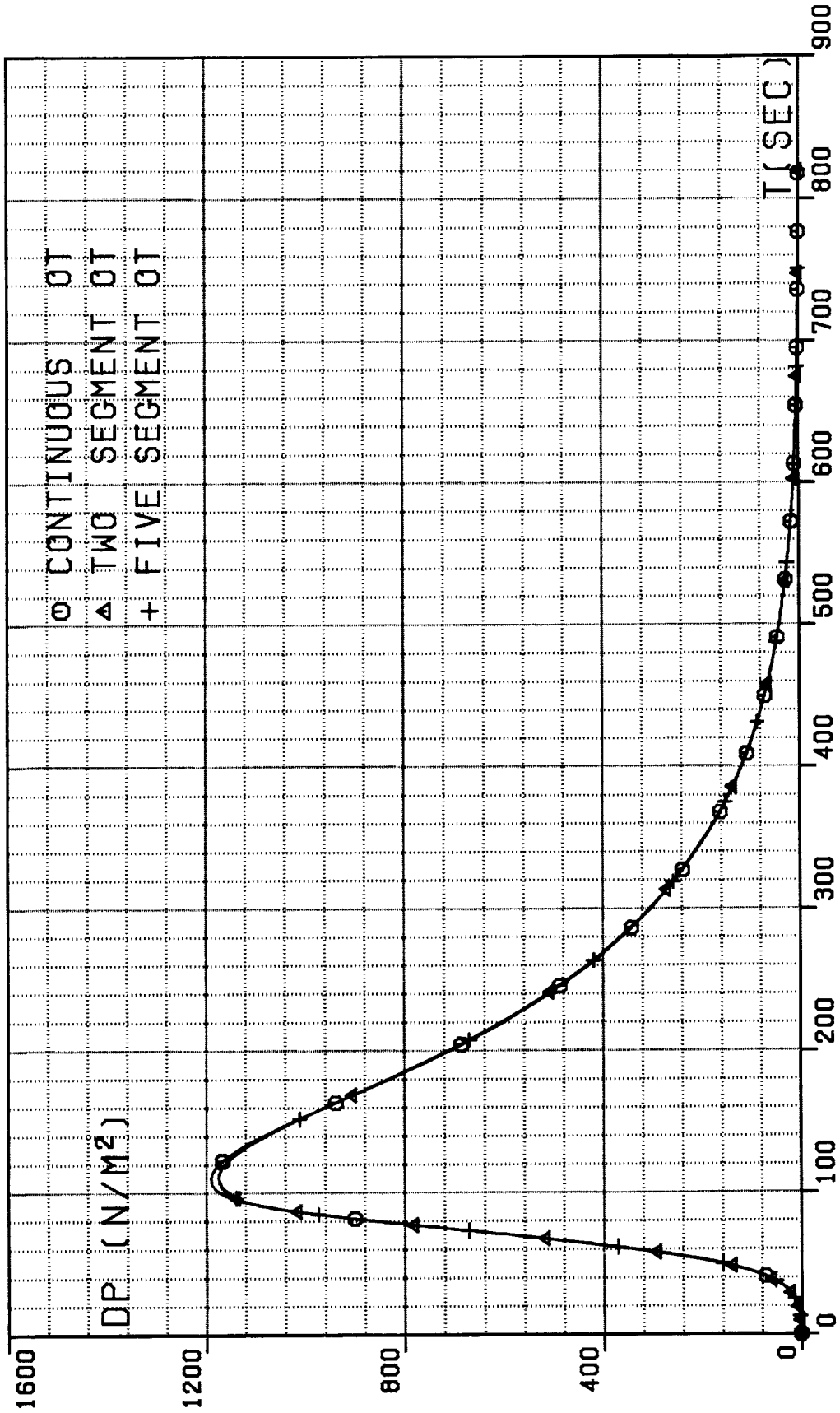
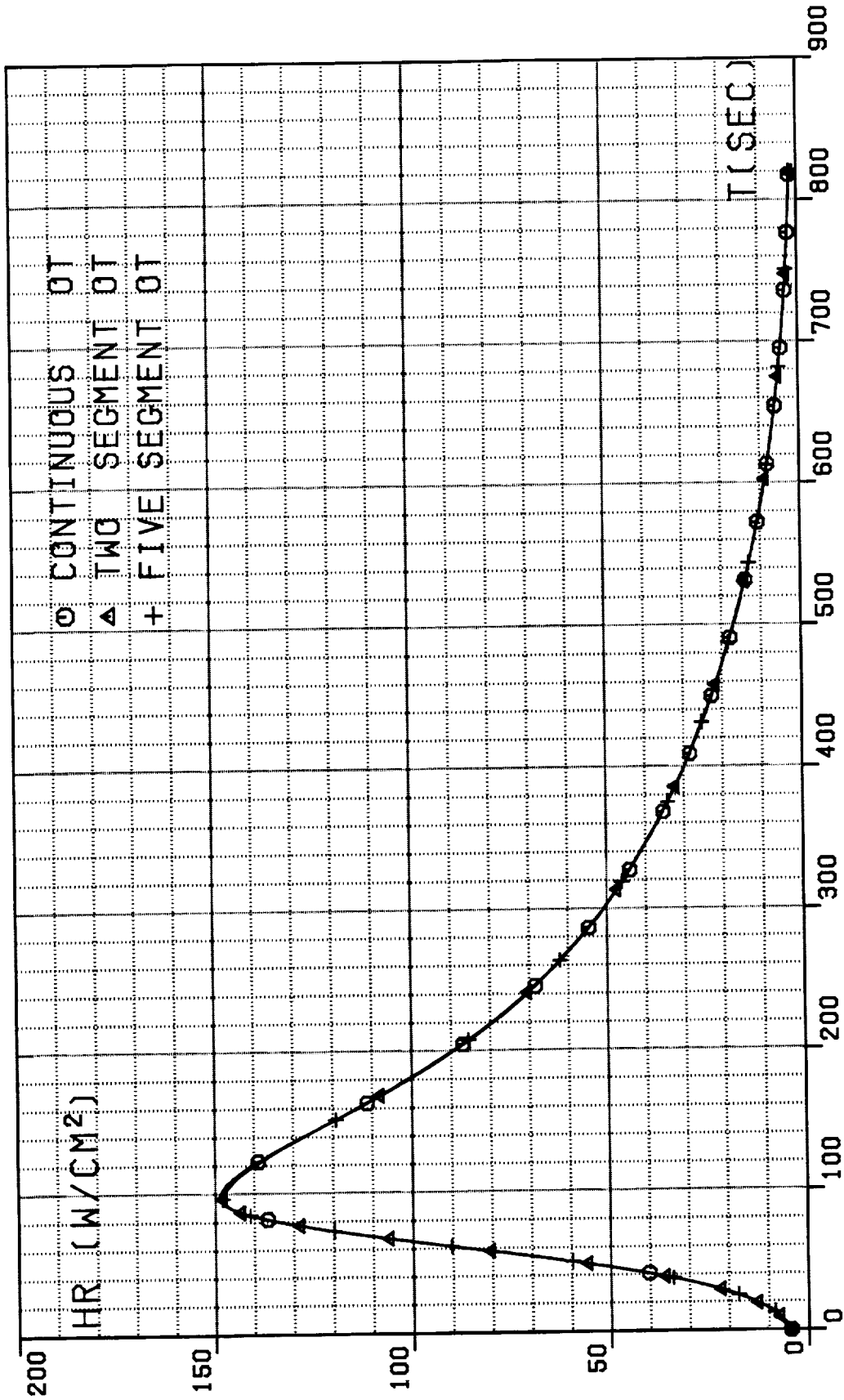FIG.2E. COMPARISON OF AFE TRAJECTORIES,
TRANSFER (DA), DYNAMIC PRESSURE.

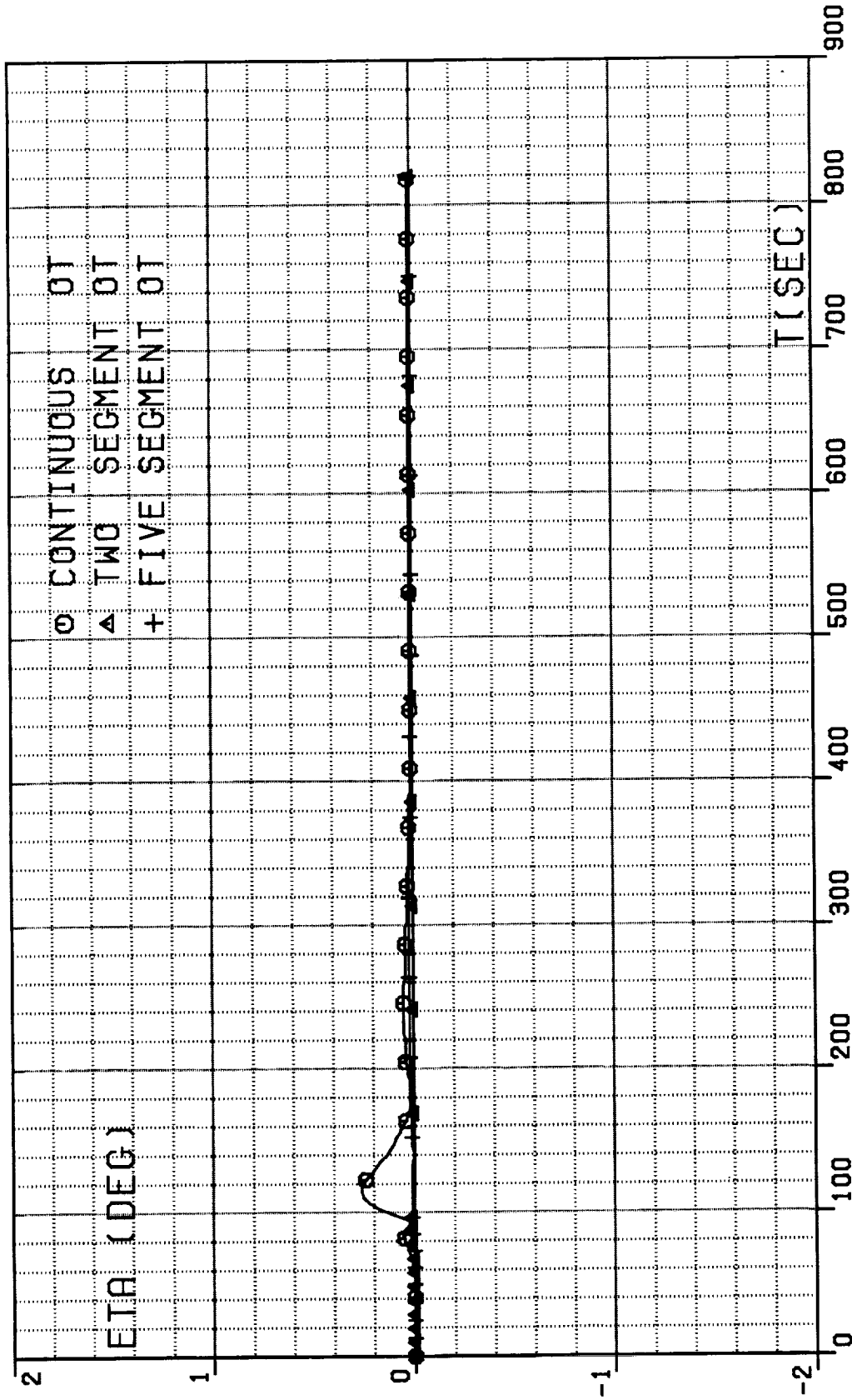FIG.2F. COMPARISON OF AFE TRAJECTORIES, TRANSFER (DA), HEATING RATE.

FIG.2G. COMPARISON OF AFE TRAJECTORIES,
TRANSFER (DA), WEDGE ANGLE.

Abstract. ~~This report is the third of a series (Refs. 1-4)~~ *stat* ~~dealing with the determination of optimal trajectories for the aero-~~ *is investigated in this report* assisted flight experiment (AFE). The intent of this experiment is to simulate a GEO-to-LEO transfer, where GEO denotes a geosynchronous Earth orbit and LEO denotes a low Earth orbit. ~~Specifically, the AFE spacecraft is released from the space shuttle and is accelerated by means of a solid rocket motor toward Earth, so as to achieve atmospheric entry conditions identical with those of a spacecraft returning from GEO. During the atmospheric pass, the angle of attack is kept constant, and the angle of bank is controlled in such a way that~~ (the following conditions are satisfied: (a) the atmospheric velocity depletion is such that, after exiting, the AFE spacecraft first ascends to a specified apogee and then descends to a specified perigee; and (b) the exit orbital plane is identical with the entry orbital plane.) The final maneuver, not analyzed here, includes the rendezvous with and the capture by the space shuttle.

~~In this report,~~ the trajectories of an AFE spacecraft are analyzed in a 3D-space, employing the full system of 6 ODEs describing the atmospheric pass. The atmospheric entry conditions are given, and the atmospheric exit conditions are adjusted in such a way that ~~requirements (a) and (b) are met, while simultaneously minimizing~~ the total characteristic velocity, *and* hence the propellant consumption required for orbital transfer *are minimized.* Two possible transfers are

considered: (IA) indirect ascent to a 178 NM perigee via a 197 NM apogee; and (DA) direct ascent to a 178 NM apogee.

For both transfers, two cases are investigated: (i) the bank angle is continuously variable; and (ii) the trajectory is divided into segments along which the bank angle is constant. For case (ii), the following subcases are studied: two segments, three segments, four segments, and five segments;because the time duration of each segment is optimized, the above subcases involve four, six, eight, and ten parameters, respectively.

In the analytic conclusion, ~~A surprising result of the analysis is that~~ the optimal trajectories of cases (i) and (ii) are shown to coalesce into a single trajectory: a two-subarc trajectory, with the bank angle constant in each subarc ~~(bang-bang control)~~. Specifically, the bank angle is near 180 deg in the atmospheric entry phase ~~(positive lift projection phase)~~ and is near 0 deg in the atmospheric exit phase ~~(negative lift projection phase)~~. ~~Another surprising result is that,~~ during the atmospheric pass, the peak values of the changes of the orbital inclination and the longitude of the ascending node are nearly zero; hence, the peak value of the wedge angle (angle between the instantaneous orbital plane and the initial orbital plane) is nearly zero. This means that the motion of the spacecraft is nearly planar in an inertial space.

The guidance implications of the above results are discussed.

Key Words. Flight mechanics, hypervelocity flight, atmospheric flight, optimal trajectories, aeroassisted flight experiment, aeroassisted orbital transfer, guidance.